A new analytical approach for describing fatigue load sequence effects

R.C. Dragt [1], S.T. Hengeveld [2], J. Maljaars [2, 3]

[1] Department of Structural Dynamics, Institute for Applied Scientific Research (TNO), Delft, the Netherlands

[2] Department of Structural Reliability, Institute for Applied Scientific Research (TNO), Delft, the Netherlands

[3] Structural Design, Department of the Build Environment, Eindhoven University of Technology Eindhoven, the Netherlands

Load sequence effects in fatigue crack growth, such as retardation and acceleration due to a large overload (OL) and underload (UL), can dramatically change the (remaining) fatigue life. These effects can be determined using analytical and numerical tools, often trading accuracy for a steep increase in required calculation time. This paper describes a novel analytical model that includes these load sequence effects, with reasonable accuracy and with significantly less computation time as compared to numerical tools. This analytical description is based on observations from numerical simulation and fatigue crack growth experiments. The model uses simple and scalable equations for the OL effect on the crack openings stress. It also accounts for the effect of very low stress valleys, ULs, that can (partly) cancel this effect. This UL effect is treated independently of the OL. This adopted modular approach provides the model with the required flexibility to describe (semi-) variable amplitude signals. The model is calibrated with a set of experiments and compared against the experimental results and analytical models from literature.

Keywords: Fatigue, load sequence effects, overloads, underloads, crack growth, offshore wind turbines

1 Introduction

In offshore wind turbine (OWT) substructure design, fatigue damage estimations are usually made using the Palmer-Miner rule of linear cumulative damage. While this approach considers the contribution of both small and large stress cycles to the total

estimated damage, it does not consider load sequence effects. It is experimentally observed that the crack growth rate of small cycles reduces when they have been preceded by a relatively large stress cycle, called an overload (OL). This is, for example, illustrated by the experimental results by (Maljaars et al., 2015), see Figure 1. This figure shows the crack growth versus the number of cycles. The loading signal consists of constant amplitude (CA) loading with a four OLs, as indicated by the arrows. The experimental results show lower crack growth rates for the CA cycles following each of the OLs, a phenomenon called crack retardation. This behaviour is experimentally shown for various materials, for example aluminium (Yisheng and Schijve, 1995) and steel (Maljaars et al., 2015).

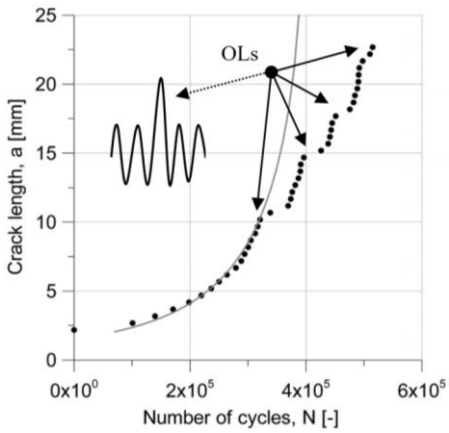

Figure 1: Crack length as a function of the number of cycles. The loading signal consists of CA loading with one OL. The dotted line represents the test results, the grey line a simulation not taking OL effects into account. Figure taken from Maljaars et al. (2015).

However, a loading signal consisting of solely CA and a single OL loading is not representative for the complex stress histories that OWT structures experience. A realistic load pattern is random with a certain bandwidth, and in this paper referred to as Variable Amplitude (VA) loading. The effect that load sequences can have on the fatigue life of OWT substructures subjected to VA loading has been investigated in the joint industry project "Fatigue life Load Sequence effects and Failure probability driven Inspection" (FeLoSeFI). This project aimed to understand the effects of load sequences and to develop models for the estimation of the load sequence dependent fatigue damage in order to optimize maintenance intervals. Dedicated finite element models have been developed to understand the mechanics governing the retardation and acceleration effects. However

accurate, these models also come with substantial calculation times, making them impractical for engineering assessments. Therefore, a novel fracture mechanics model is developed to estimate the crack growth including load sequences, consisting of analytical equations only. The developed model improves on accuracy and flexibility when compared to existing analytical models and requires significantly less computation time as compared to numerical models. This paper describes the complete version of this model. Earlier work describing parts of the model has been published in (Dragt et al., 2016, 2017, 2018).

1.1 Behaviour after an OL

Various explanations for the crack growth behaviour after an OL exist in literature. Anderson (2017) provides a summary of the three main explanations. These are summarized below and schematically shown in Figure 2.

1. The first concept is based on the creation of a plastic zone by the OL, which is located in front of the crack tip. This plastic zone contains residual stresses which reduce the effective stress of the subsequent, smaller amplitude. This effect is present as long as the crack is within the plastic zone. This mechanism is called the plastic zone concept.

2. The second concept is based on a plastic wake along the flanks of the crack tip. This plastic wake increases the stress required to open the crack and thereby reduces the crack growth rate of subsequent cycles. This concept is called the plasticity induced crack closure concept.

3. The final concept states that the crack blunts after an OL and needs to re-sharpen or re-initiate, thereby slowing the crack growth rate after the OL.

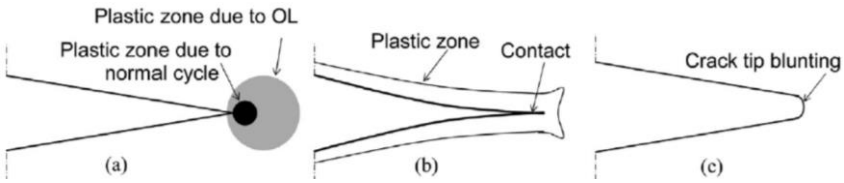

Plastic zone ahead of crack tip *Plastic zone at crack flanks* *Crack tip blunting*

Figure 2: Schematic presentations of retardation concept (Maljaars et al., 2015)

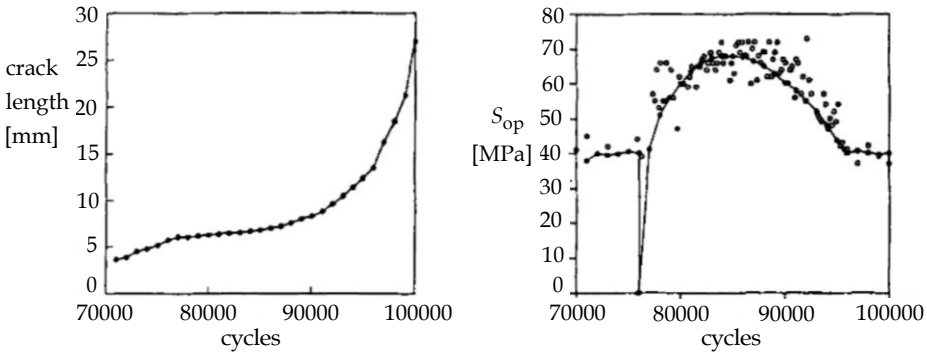

Figure 3: Effect of an OL on the crack growth (left) and the opening stress (right). The signal consists of CA loading (S_{max} = 100 MPa, S_{min} = 0 MPa) with an OL (S_{max} = 200 MPa) (Yisheng and Schijve, 1995).

The OL effect is most likely a combination the effects described above, but the plasticity induced crack closure is often mentioned as being the most important contributor (Anderson, 2017). This mechanism is the basis of the remainder of this paper.

The plasticity induced crack closure concept is based on the definition of the opening stress S_o , which represents the threshold stress above which the crack physically opens. Stresses up to S_o are assumed not to contribute to the fatigue damage during that cycle. Experiments with CA loading and discrete OLs have shown that the crack opening stress after an OL first drops, after which it increases to its maximum value and slowly decays back to the normal CA value, see Figure 3 (right). This figure shows the crack opening stress over the number of cycles, with the OL applied around 76,000 cycles. The left side of the figure shows the corresponding crack length, over the number of cycles. This figure also shows the reduced crack growth rate after the OL is applied.

The relative size of the OL compared to the CA cycles, the OL-ratio (S_{maxOL} / S_{maxCA}), is a key influence factor for retardation, as has been shown by Ding et al. (2017). Higher OL ratios induce more severe retardation effects. Furthermore, Yuen and Taheri (2006) reported that multiple OLs, relatively close to each other, increase the retardation effect. Too close, however, will decrease the total retardation effect, as the initial acceleration outweighs the retardation effect.

1.2 Influence of underloads

The application of a large load valley, or Underload (UL), may reduce or cancel out the retardation effect of a preceding OL. The mechanism is as follows: The large load valley reduces the compressive stress in front of the crack tip (plastic zone concept) and/or the flattening of the plasticity induced bulging in the crack wake (plasticity induced crack closure concept). Finally, when a UL is applied in a CA signal (without preceding OL), acceleration can be seen, but the effect is much smaller than the retardation following the OL (Ding et al., 2017). The net retardation or acceleration effect of OLs and ULs is highly dependent on the sequence of cycles with OLs and ULs, their relative size (e.g. the OL-ratio) and subsequent cycles.

2 Fracture mechanics models

Fracture mechanics methods enable the determination of the crack length, based on every loading cycle experienced and the current (updated) size of the crack. As this method requires a given crack length, the process of crack initiation is not taken into account and (small) initial cracks are assumed to be present at the start of the process. This is a valid assumption for welded structures, as the welding process itself introduces small defects in the structure. This section gives an overview of the governing equations and provides a number of variants on the basic fracture mechanics method. First, the Linear Elastic Fracture Mechanics (LEFM) theory is explained, as this is the basis of many fracture mechanics models. This theory, however, does not take retardation or acceleration effects into account. Therefore, the Willenborg model and the State-Space model that enable retardation to be considered, are subsequently introduced.

2.1 Linear Elastic Fracture Mechanics

The LEFM method states that the crack growth is governed by stress intensity factor, K, which describes the local stress field near a crack tip. Equivalently to a stress range ($\Delta S = S_{max} - S_{min}$), ΔK can be defined as a range, see Equation 1.

$$\Delta K = K_{min} - K_{max} = Y(S_{max} - S_{min})\sqrt{\pi a} \tag{1}$$

In this equation, S_{min} and S_{max} are the minimum and maximum stress, respectively, describing the current stress cycle, a is the current crack size and Y is the geometry correction factor. Several methods exist to determine Y, for example by use of finite

element analysis or, for specific geometries, through empirical formulations. In this work, an empiric geometric correction factor for a SENB4 bending specimen according to Tada et al. (1973) is used, see Equation 2.

$$Y = \frac{0.923 + 0.199(1 - \sin\phi)^4}{\cos\phi}\sqrt{\frac{\tan\phi}{\phi}} \tag{2}$$

In which $\phi = \pi a/(2W)$ and W is the width of the specimen. The actual crack growth per cycle, da/dn, is described by Paris (1964) as a function of the stress intensity range, ΔK and the material specific parameters C and m. The simple crack growth relation used is given in Equation 3 and features a threshold stress intensity range, ΔK_{th}, below which there is no crack growth.

$$\frac{da}{dN} = \begin{cases} 0 & \text{if } \Delta K \le \Delta K_{th} \\ C(\Delta K)^m & \text{if } \Delta K > \Delta K_{th} \end{cases} \tag{3}$$

In addition, Elber (1971) showed that the ratio of minimum to maximum stress ($R = S_{min} / S_{max}$) further influences the crack growth. Therefore, the variables C and ΔK_{th} are also stress cycle dependent.

2.2 *Small scale plasticity and the concept of crack opening*

The above mentioned equations are valid for LEFM as they assumes a singular stress field at the crack tip. In metals, however, local plasticity can change this stress field and cause the crack to remain (partly) closed during part of the loading cycle. This is modelled by the concept of the stress opening stress S_o. Stresses lower than S_o are assumed not to contribute to the fatigue damage during that cycle. Elber (1971) states that the remaining part of the stress cycle is contributing to the fatigue crack growth and is called the effective stress range, $\Delta S_{eff} = S_{max} - S_o$. This concept is schematically shown in Figure 4, where S_{min}, S_{max}, and S_o are shown. These define the stress cycle ΔS and effective stress cycle ΔS_{eff}. Generally speaking, a higher stress ratio R leads to less plasticity and reduces the difference between S_o and S_{min}. Consequently, this leads to a higher crack growth rate. This can be incorporated by the effective stress intensity range, ΔK_{eff}:

$$\Delta K_{eff} = U\Delta K \tag{4}$$

In which the effect of plasticity is accounted for by the stress range effectivity ratio, U, see Equation 5.

$$U = \frac{S_{\max} - S_o}{S_{\max} - S_{\min}} \tag{5}$$

Incorporating ΔK_{eff}, instead of ΔK, in Equation 3 has the advantage that C and ΔK_{th} are then material dependent variables, i.e. not related to R. The problem is now reduced to finding the material and ratio dependent variable U. This can be done by using empirical data for CA loading or through use of detailed finite element models.

A commonly used empirical method adopted to estimate U is the Forman-Mettu relationship, see Equations 6 - 8 (Koçak et al., 2008). These equations relate the crack opening function, f, to $S_{\min}$, $S_{\max}$, the constraint factor α and the yield stress σ_y.

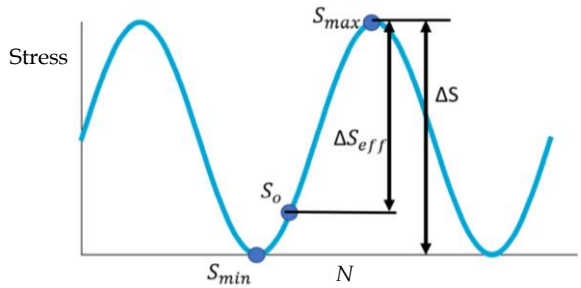

Figure 4: Schematic stress cycle showing $S_{\min}$, $S_{\max}$ and S_o as well as the stress ranges ΔS and effective stress range ΔS_{eff}

$$\begin{aligned}
A_0 &= (0.825 - 0.34\alpha + 0.05\alpha^2)\left(\cos\frac{\pi S_{max}}{2\sigma_y}\right)^{\frac{1}{\alpha}} \\
A_1 &= (0.415 - 0.071\alpha)\frac{S_{\max}}{\sigma_y} \\
A_2 &= 2 - 3A_0 - 2A_1 \\
A_3 &= 2A_0 - A_1 - 1 \\
f_1 &= A_0 - A_1 R + A_2 R^2 + A_3 R^3 \\
f_2 &= A_0 + A_1 R \\
f &= \begin{cases} \max(0, R, f_1) & R \geq 0 \\ \max(0, f_2) & R < -2 \\ \max(0, A_0 - 2A_1) & \text{else} \end{cases}
\end{aligned} \tag{6}$$

Equations 7 and 8 describe the determination of S_o and U.

$$S_o = f S_{\max} \tag{7}$$

$$U = \frac{1-f}{1-R} \tag{8}$$

The crack growth rate is then determined using Equation 9:

$$\frac{da}{dN} = C(U\Delta K)^m \frac{(1-\frac{\Delta K_{\text{th}}}{\Delta K})^p}{(1-\frac{\Delta K_c}{\Delta K})^q} \tag{9}$$

Equation 9 determines the crack growth rate per cycle da/dN, as a function of empirical material parameters C, m, p and q. They are obtained through curve fitting of CA crack growth tests. The stress intensity factor ΔK_c is the critical stress intensity factor at which failure occurs. The final term in Equation 9 describes the near threshold crack growth behaviour through the ratio $\Delta K_{\text{th}} / \Delta K$ and the near failure behaviour through the ratio $\Delta K_c / \Delta K$. Combining Equations 7-9 shows that an increase in openings stress S_{o} results in a decrease in crack growth rate, as expected.

2.3 Willenborg model

The plastic zone concept (see Figure 2a) is the basis of the Generalized Willenborg model Willenborg et al. (1971); Gallagher (1974). This simple analytical model predicts the retardation effect of an OL as a function of the size of the plastic zone in front of the crack tip. For each subsequent cycle of which the plastic zone is within this large plastic zone, a compressive stress intensity factor is considered which reduces the effective cycle. This means that the crack growth rate reduces. Once the plastic zone of a cycle exceeds the plastic zone of the OL, the original steady state crack growth is obtained. Although computational inexpensive, the Generalized Willenborg model is only able to include the effect of discrete OLs. The cancellation effects seen by ULs is not included and neither are the concepts of initial acceleration and delayed retardation. However, the model is still adopted as reference case in the current paper because of its wide application.

2.4 State-Space Model

Ray and Patankar (2001) have developed the State-Space model, which aims to include the effects of OLs and ULs in a computationally inexpensive way. The model is based on the plasticity induced crack closure approach (see Figure 2b) and treats the opening stress, S_{o}, and the current crack length, a, as state variables. In the State-Space model, S_{o} is a function of the current cycle and the stress history.

Different from the definition given in Figure 4, the State-Space model defines a stress cycle as the maximum stress, $S_{\max}$, and its following (instead of preceding) minimum stress, $S_{\min}$. The opening stress in the K_{th} cycle is determined by:

$$S_o^k = \frac{1}{1+\eta} S_{\text{o}}^{k-1} + \frac{\eta}{1+\eta} S_{\text{oCA}}^k + \frac{1}{1+\eta}(S_{\text{oCA}}^k - S_{\text{o}}^{k-1}) \cdot H(S_{\text{oCA}}^k - S_{\text{o}}^{k-1}) + \\ + \frac{1}{1+\eta}(S_{\text{oCA}}^k - S_{\text{oCAp}}^k) \cdot H(S_{\min}^{k-1} - S_{\min}^k)[1 - H(S_{\text{oCA}}^k - S_{\text{o}}^{k-1})] \tag{10}$$

Where, η is the decay factor describing the decay of the retardation effect. The opening stress of the current cycle is a function of the opening stress of the previous cycle, S_{o}^{k-1} , the opening stress for the current CA loading, S_{oCA}^k and two Heaviside functions, $H()$, to allow for the quick rise and slow decay of the opening stress (third term) and the cancellation effect by ULs (fourth term). The latter includes the openings stress of the previous cycle, which is determined using $R = S_{\min}^{k-1} / S_{\max}^k$.

The state-space model does describe the retardation, initial acceleration and cancellation effects. However, the latter is only the case when the UL directly follows the OL, which is an important limitation to the State-Space model as this restricts the approach from capturing realistic VA loading signals. This model is used as a second reference case in this paper.

3 New 'SECOD' Model

A new Simple Equation based Crack Opening Determination (SECOD) model is developed in this paper to estimate the fatigue crack growth, including the effects of OLs and ULs. The model is created such, that it is suited for realistic (semi)-VA loading with an improved accuracy over other existing simple models, such as the State-Space model. The SECOD model is based on the principles of plasticity induced crack closing, as discussed in Section 2. The model is inspired by the State-Space model and uses the same concept of state variables to describe the effect of stress history on the current crack growth rate. The model is semi-empirical in nature and is calibrated based on a set of tests, which are briefly described in Section 5.

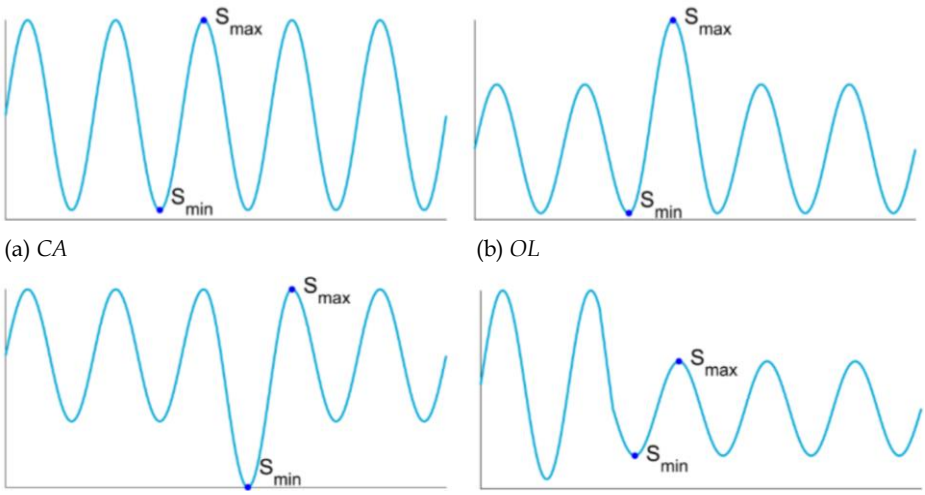

(a) *CA* (b) *OL*

(c) *UL* (d) *Mean change*

Figure 5: Considered cyclic loading conditions

The SECOD model uses a basic stress cycle description, as described in Section 2 and Figure 4, and incorporates the Forman-Mettu approach to determine the opening stress, see Equations 6-8. As these equations describe the crack opening stress in CA loading they receive the subscript ss (steady state).

The effect of OLs and ULs on subsequent cycles is captured by modifying the opening stress by a factor ΔS_o , see Equation 11. Finally, the crack growth rate is determined using equations 8 and 9.

$$S_o = S_{oss} + \Delta S_o \tag{11}$$

*3.1 **Modular approach***

The opening stress S_o changes constantly in a VA load, depending on the plastic wake that has been formed by preceding cycles. The main challenge is to find the appropriate values for ΔS_o . This requires a level of flexibility which is included through a modular approach, where four types of cyclic loading are specified: a) CA loading, b) OL, c) UL and d) mean change. These four types are shown schematically in Figure 5. By combining these four types, e.g. an OL and mean change at the same time, every type of loading sequence one might encounter in VA loading can be described. This also means that a new event may be introduced before the effect of a previous event is completely decayed. The following combinations are described later in this paper:

- An OL results in retardation of the crack growth due to the effects described in the previous sections. An UL can cancel the effect of an OL, thereby reducing the amount of retardation. Furthermore, it is assumed that a single UL (with no preceding OL) does not induce acceleration.
- Overlapping OLs can have a combined retardation effect.
- If an OL is followed by more than one UL, subsequent ULs further reduce retardation.
- A mean change, see Figure 5(d), is considered as a change in stress ratio and/or range, combined with an OL and/or UL. The latter depends on whether the values for S_{min} and S_{max} shift up or down.

The SECOD model as described here is flexible enough to process a variable amplitude signal and track the load sequence effects.

4 Step by step description

In this section, the SECOD model is described step-by-step. Figure 6 shows a summary of the model. It exists of eight steps which will be discussed in detail in the following subsections. The presented scheme is used for every single stress cycle in the loading history, in a cycle-by- cycle crack growth calculation. The procedure starts with the initiation of a new cycle in block 1. Block 2 checks whether or not the cycle is fully in compression. The effect of a possible OL, UL and mean change is determined in blocks 3, 4 and 5. Next, block 6 determines the crack growth of the current cycle. In parallel, block 7

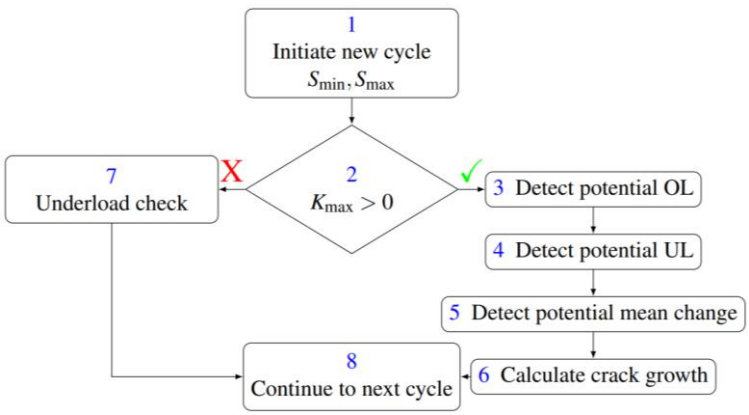

Figure 6: Flowchart of the complete model

determines whether or not the compressive cycle is an UL. Finally, block 8 saves the state variables and finishes the current cycle. In the following subsections, the working of the model and the rationale behind the modelling choices are explained. The flowcharts show the equations in rectangular shapes and choices are represented by diamond shapes.

Block 1: Initiating a new cycle

For a new cycle, the far field minimum stress S_{min} and the subsequent (far field) maximum stress S_{max} of the cycle are determined. Based on the workflow explained in Section 2, the current length of the crack, a, and the geometry factor Y, the stress intensity factors K_{min} and K_{max} are determined, using Equations 1 and 2.

Block 2: Is the cycle in tension?

The assumption is made that a completely compressive cycle, i.e. $K_{max} < 0$, does not result in crack propagation. Therefore, no further crack growth increment is calculated and blocks 3-6 are not executed. A completely compressive cycle can be an UL, however, so the workflow continues to the UL-check in block 7.

Block 3: Detecting potential OL

This subsection describes the detection of an OL and the implementation of the OL effect. This is one of the most important parts of the model and contains several choices to account for the various scenarios that can occur in VA loading. This subsection starts with a basic description of the OL model and the underlying assumptions. Next, the SECOD implementation is described.

The OL effect

The implementation of the OL effect is based on the general behaviour after an OL, as visualized by Anderson (2017) in Figure 7. This figure shows the crack growth rate per cycle as a function of the distance from the OL, which accelerates directly after the OL. This is followed by a longer period of crack growth retardation.

The OL behaviour is modelled numerically by Voormeeren et al. (2017) using the Thick Level Set method. This method is used to gain insight into the shape of the retardation zone, as well as in the magnitude of retardation over a range of OLs and R-ratios. Furthermore, the effect of applying a second OL, within the retardation zone of the first OL was investigated.

For this paper, SENB4 specimens (as described in Section 5) with an initial crack are modelled. The plane strain model uses a S355 steel description that includes both isotropic and kinematic hardening. The material parameters are taken from Nip et al. (2010) and have also been used as input for other finite element analyses within the FeLoSeFI project, as described by Maljaars and Tang (2019). The model itself is explained in detail in Voormeeren et al. (2017). As for the application in the current paper, the model itself and input parameters remain similar to the description in the paper, the load cases are new as to include the OLs and ULs at various distances.

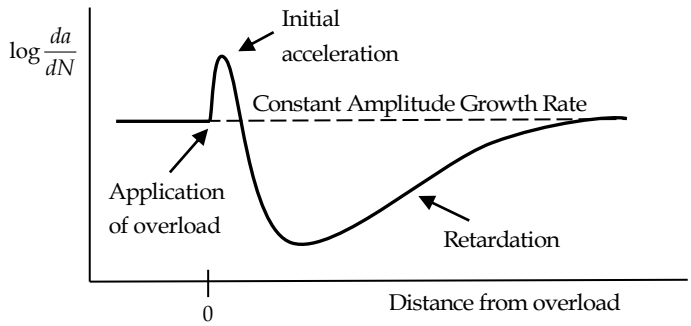

Figure 7: Crack growth rate versus distance after application of an OL
Redrawn after Anderson (2017)

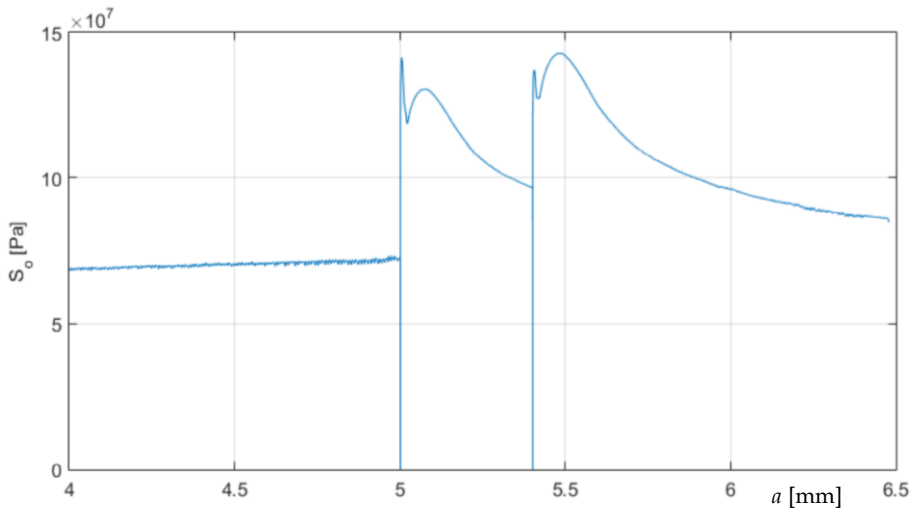

Figure 8: S_o versus a, as calculated with the Thick Level Set method
(Voormeeren et al., 2017)

For the creation of the SECOD model, the evolution of S_o after an OL event is of particular interest. Next to variations of CA loading with a single OL, also overlapping OL events are modelled. For example, figure 8 shows the effect of two overlapping OLs in terms of the opening stress, S_o , versus the crack size a. The loading signal consists of CA loading (S_{min} = 65 MPa, S_{max} = 216 MPa and R = 0.3) with two OLs (S_{min} = 65 MPa, S_{max} = 367 MPa) applied at a = 5 mm and 5.4 mm. The figure shows the initial acceleration due to the decrease of S_o and de delayed retardation that follows. It also shows that the influence of the second OL is only slightly larger than that of the first, even though S_o is still elevated due to the first OL.

Based on observations from literature and the numerical variation study, the following three governing assumptions drive the OL effect within the SECOD model:

- The OL effect results from the plasticity induced by a relatively large loading cycle, when compared to subsequent stress cycles. Therefore, the magnitude of the OL effect is solely dependent on the height of the OL, which is captured by the maximum stress of the cycle, S_{max} , relative to the height of the preceding cycle, S_{max}^{prev} .
- The length of the influence zone of an OL is dependent on the magnitude of the OL and is assumed to scale with the size of the plastic zone.
- The OL effect ΔS_o has a predefined shape, which scales with the magnitude of the OL effect and length of the influence zone, as described above.

An OL is triggered on hindsight. Hereby, it is assumed that in a cycle-by-cycle approach, information is available on the previous cycle (history), but not always on the future cycles (e.g. in real-time analyses) So, at the current cycle, an OL at the previous cycle is triggered when two conditions are met: *a)* the maximum stress of previous cycle, S_{max}^{prev} is higher than the S_{max} of the current cycle, and *b)* the opening stress S_o^{prev} of the previous cycle is higher than the current S_o . The first condition triggers a possible OL effect at previous cycle and the second condition checks whether the induced plasticity of the OL is larger than the plasticity currently present. If this is not the case, it means that an earlier OL is still dominant. The latter is important in VA loading, otherwise every slightly larger cycle would trigger a new OL effect.

After an OL, S_o decreases which results in an initial crack acceleration, similar to the effect described in Figure 7. This decrease is realized by an initially negative ΔS_o . When the crack grows, ΔS_o slowly increases to maximum value, $\Delta S_{o\,peak}$. At this point, the OL effect

is at its maximum. Afterwards, ΔS_o decays to $\Delta S_o = 0$ using a power law. The length of the OL effect zone, r_{OL}, scales with the magnitude of the OL. Equations 12 and 13 describe the function for ΔS_o due to the OL.

$$\Delta S_o = \Delta S_{o\,peak} \cdot \min(\tau_1, \tau_2) \tag{12}$$

in which

$$\begin{aligned} \tau_1 &= (1 + c_{acc})\left(\frac{x}{x_{top}}\right)^{c_{\tau 1}} - c_{acc} \\ \tau_2 &= \left(1 + c_{top} - \frac{x}{x_{top}}\right)^{c_{\tau 2}} \end{aligned} \tag{13}$$

In these equations, c_{acc}, $c_{\tau 1}$ and $c_{\tau 2}$ are fitting constants describing the magnitude of initial acceleration and the increase and decrease of the retardation effect. The length of the OL influence zone is inspired by the equation by (Toribio and Kharin, 2013) for the plastic zone size:

$$r_{OL} = 0.14 \frac{K_{max}(K_{max} - K_{min})}{S_y^2} \tag{14}$$

The maximum opening stress, $\Delta S_{o\,peak}$ occurs at distance x_{top}, which is fitted according to $x_{top} = c_{top}\, r_{OL}$ using numerical simulations. All distances x are measured from the a_{OL}, which represents the crack length when the OL event takes place, see Figure 9.

$\Delta S_{o\,peak}$ is a function of S_{max} of the OL and S_{max} of the following cycle. Evaluating the experiments, it is observed that both the difference between, and the ratio of, maxima influence the value of $\Delta S_{o\,peak}$. These effects are captured in Equation 15, in which c_1 and c_2 are (experimentally and numerically) calibrated coefficients.

$$\Delta S_{o\,peak} = (c_1 + c_2 (\frac{S_{max}^{OL}}{S_{max}} - 1))(S_{max}^{OL} - S_{max}) \tag{15}$$

Finally, the OL effect is assumed present as long as: The crack has not grown outside of the OL influence zone ($a \leq (a_{OL} + r_{OL})$ and ΔS_o has not decayed to zero. The implementation of the OL, as discussed in this paragraph is shown schematically in a flowchart (Figure 10). The following paragraphs will discuss the blocks one-by-one. Again, the paragraph numbering refers to the numbers in the blocks.

Block 3

Block 3.1: Calculating the stresses, stress intensities stress range affectivity ratio

In this block, the stress ratio, R and the stress intensity factors K_{min} and K_{max} (see Equation 1) are calculated. Furthermore, both the stress range effective ratio U (see Equation 8) and the opening stress S_o (see Equation 7) are determined. As future stresses are not yet known, these are now treated as steady state (assuming the rest of the signal consist of similar VA cycles) and receive the subscript ss.

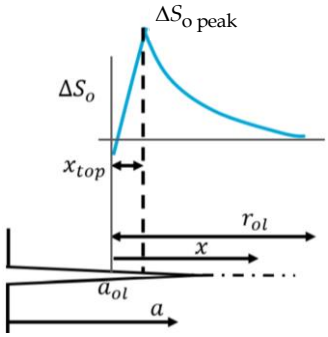

Figure 9: Schematic representation of the change in ΔS_{ok} after an OL applied at a_{OL}

The value $\Delta S_{o\ peak}$ is determined, assuming that the previous cycle was indeed an OL, with respect to the current cycle. As this assumption is checked later, it is treated as a temporary value: $\Delta S^{temp}_{o\ peak}$, see Equation 16. Physically speaking, a plastic zone is created which is larger than the plasticity currently present, and therefore governs the crack growth behaviour from here on forwards.

$$\Delta S^{temp}_{o\ peak} = (c_1 + c_2 (\frac{S^{prev}_{max}}{S_{max}} - 1))(S^{prev}_{max} - S_{max}) \tag{16}$$

Block 3.2, 3.3 and 3.4: Is the current cycle in an OL influence zone?

If an OL effect is present, this is represented by the state variable ΔS^{prev}_o, which is the increase in opening stress ΔS_o from the previous cycle. ΔS^{prev}_o is used to check whether or not the current cycle is already within an OL influence zone, by comparing the state variable ΔS^{prev}_o with the potentially new OL, $\Delta S^{temp}_{o\ peak}$ (as calculated in block 3.1). When the potential new OL effect is higher than the existing opening stress, a new OL is defined. Otherwise, the current cycle is treated as a regular cycle. The blocks 3.2, 3.3 and 3.4 are explained one-by-one in the next paragraphs.

Block 3.2: Is the current cycle in an OL influence zone?

Delayed retardation is considered in the current modelling approach. During this part of the retardation zone, ΔS_o slowly increases until the peak value is reached (see Figure 9). So, if this value of ΔS_o would be used to compare with the potential new OL effect, a new OL would be defined very often, as ΔS_o is not yet fully developed. The current cycle is within the delayed retardation zone when the crack growth since the OL, x, is less than the distance to $\Delta S_{o\,peak}$, x_{top} .

Block 3.3: Is the current cycle outside of a delayed retardation zone? ($x > x_{top}$)

With the potential OL in the regular retardation regime, this decision block determines whether or not a new OL event is created. This is done when the following condition is true:

$$\Delta S_{o\,peak}^{temp} \geq \Delta S_o^{prev} \tag{17}$$

In which $\Delta S_o^{prev} = 0$ in case no OL is present. In other words, the current cycle would result in more retardation then the amount of retardation currently in the system. If so, the new OL will reset the currently present OL (ΔS_o^{prev}) and define a new retardation event purely based on this new OL. Otherwise, the currently present ΔS_o^{prev} is higher than that of the potential new OL, and the current cycle is not treated as a new event. This is an exit-condition for block 3, the routine continues assuming this cycle is a regular stress cycle. Both options are shown in Figure 11, where the lower figure shows the stress history and the upper figure describes the evolution of ΔS_o . In the left event, a new OL is created. In the right event, no new OL is started.

Block 3.4: Is the current cycle within the delayed retardation regime? ($x < x_{top}$)

In case the current cycle is within the delayed retardation area, a new OL event is defined if $\Delta S_{o\,peak}^{temp} > \Delta S_{o\,peak}$

Block 3.5: Initiating a new OL

The following steps are executed when a new OL event is introduced:

- The a_{OL} is updated to the current crack length $a_{OL} = a$.
- The minimum of the current cycle is assigned to S_{min}^{min} . This is required to later incorporate the UL effect (see block 4).
- The UL correction factor, UL_{corr} , is set to 1, thereby resetting the cancellation effect of

previous ULs.

- r_{OL} is calculated using Equation 14.
- The new OL completely replaces any OL effects currently present. Physically, additional interaction might be present. However, by resetting the retardation of the combined OLs effect is possibly (slightly) underestimated.

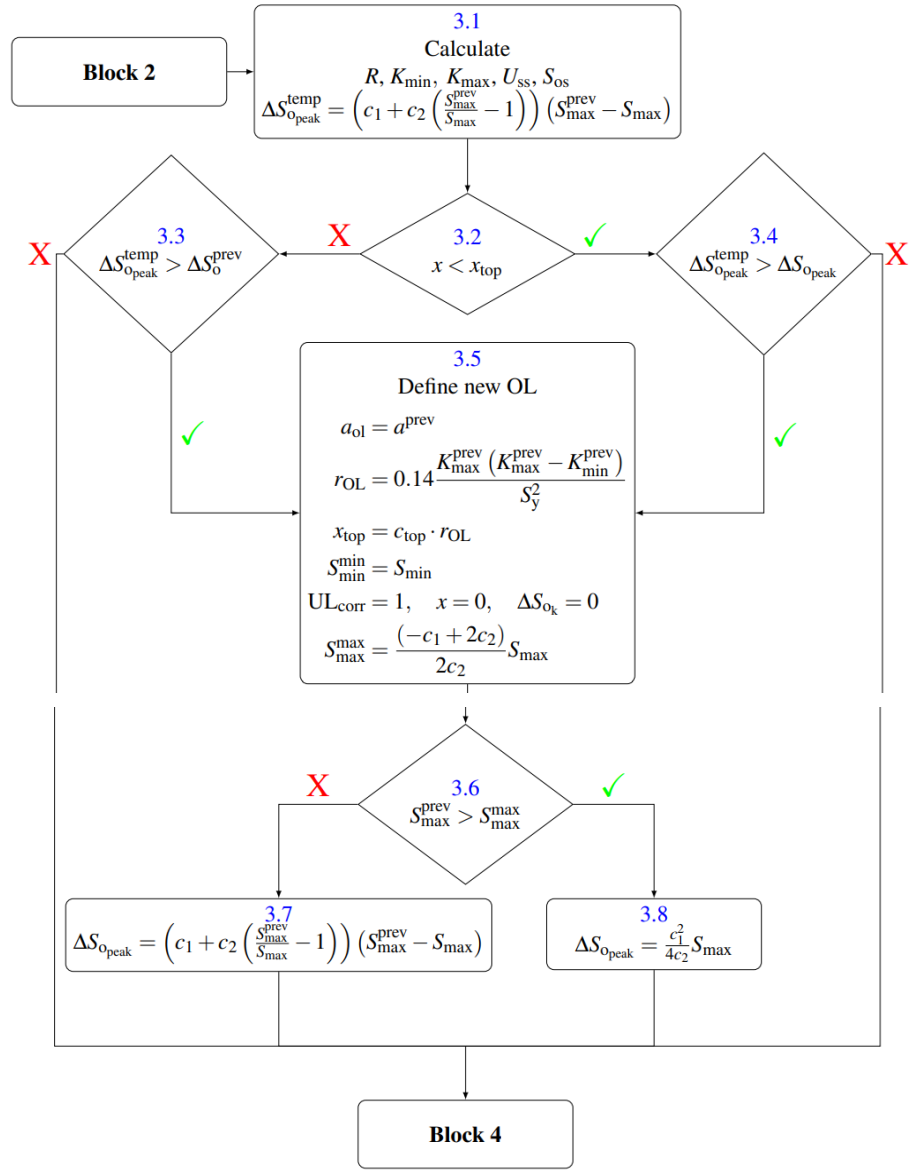

Figure 10: The implementation of an OL

Block 3.6: Is the current maximum stress above the maximum calculated stress?

Equation 15 describes the peak opening stress of the OL effect. This equation, however, is not monotonously increasing, which is shown by plotting $\Delta S_{\text{o peak}}$ as a function of $S_{\text{max}}^{\text{prev}}$ in Figure 12. This means that for very high OLs, a lower value for $\Delta S_{\text{o peak}}$ is found. This is unrealistic and avoided by taking the maximum value of Equation 15 instead. This block calculates the maximum value of Equation 15, $S_{\text{max}}^{\text{max}}$, according to Equation 18 and compares this with the maximum stress of the OL, $S_{\text{max}}^{\text{prev}}$

$$S_{\text{max}}^{\text{max}} = \frac{-c_1 + 2c_2}{2c_2} S_{\text{max}} \tag{18}$$

Block 3.7: The maximum stress is below $S_{\text{max}}^{\text{max}}$.

The value for $\Delta S_{\text{o peak}}$ is calculated with Equation 15.

Block 3.8: The maximum stress is above $S_{\text{max}}^{\text{max}}$

Combining Equations 18 and 15 gives the new description of $\Delta S_{\text{o peak}}$, representing the maximum of Equation 18 ($S_{\text{max}}^{\text{max}}$):

$$\Delta S_{\text{o peak}} = \left(\frac{c_1^2}{4c_2} + c_1\right) S_{\text{max}} \tag{19}$$

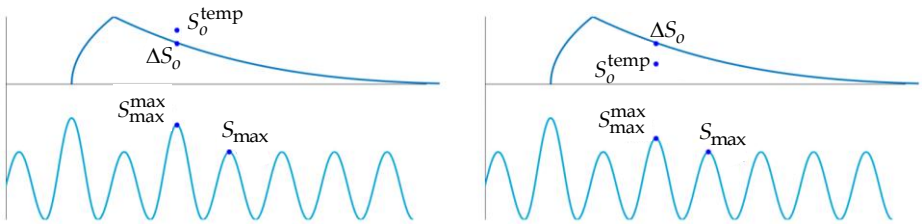

(a) *A new event is started* (b) *No new event is created*

Figure 11: Graphical representation of decision to initiate a new OL event

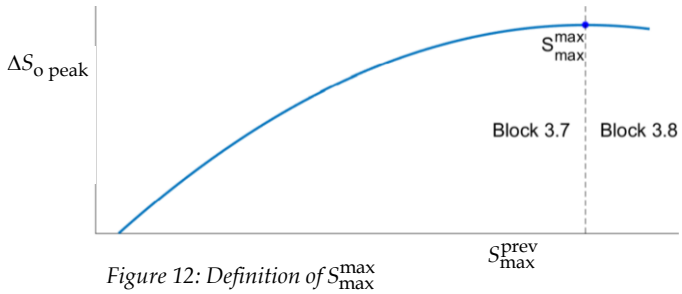

Figure 12: Definition of $S_{\text{max}}^{\text{max}}$

Block 4: Including the effect of ULs

As explained at the start of this section, an UL applied after an OL will reduce the retardation effect. This section describes the effect on an UL and how this is included in the SECOD model.

The UL effect

The UL effect has been investigated with the Thick Level Set method (by Voormeeren et al. (2017), see Subsection 4). Four SENB4 specimen (made of S355 steel) have been subjected to CA loading (S_{min} = 65 MPa, S_{max} = 216 MPa and R = 0.3) in combination with an OL (S_{min} = 65 MPa, S_{max} = 367 MPa) applied at a = 5 mm. Subsequently, a single UL (S_{min} = 0 MPa, S_{max} = 216 MPa) is applied at a = 5.01 mm, 5.1 mm and 5.2 mm respectively. The simulation results of these three cases together with a case without UL are shown in Figure 13, which provides S_o versus a. This figure shows that the magnitude of the retardation effect drops instantaneously with the application of the UL, while the length of the retardation zone remains the same.

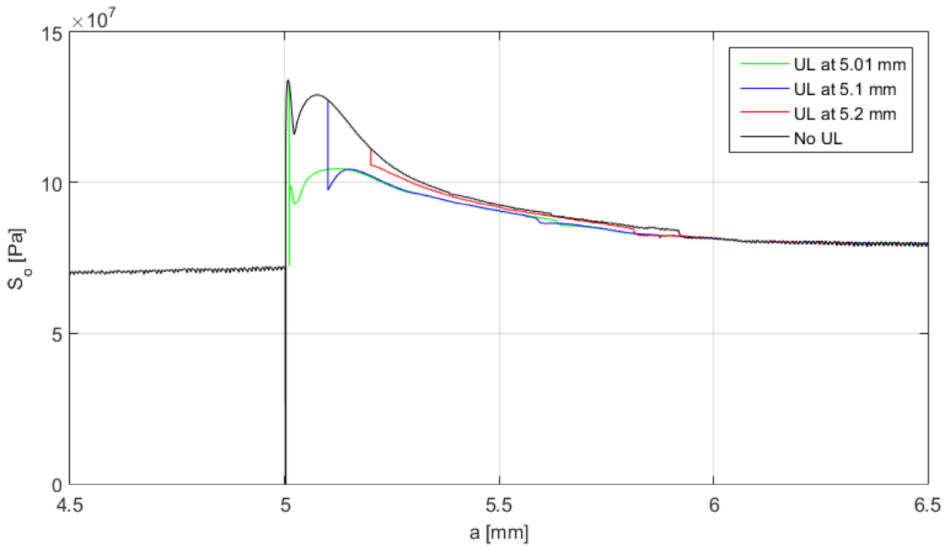

Figure 13: Opening stress versus crack length for three UL scenarios

This behaviour is included in the SECOD model through an instantaneous reduction of ΔS_o at the application of an UL. This is based on the following assumptions:

- An UL reduces the OL-effects, but does not introduce acceleration.

- An UL reduces the magnitude of ΔS_o , but does not influence the length of the OL influence zone r_{OL} .
- Multiple ULs can have a cumulative reducing effect, in case the current UL is lower than all previous ULs within the OL influence zone. This approach assumes that when the plasticity induced bulging due to an OL is flattened by an UL, it can only be flattened further by an even lower UL.

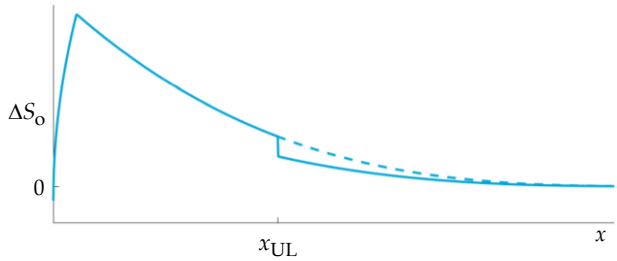

Figure 14: Schematic view of ΔS_o after an OL event with (solid line) and without UL effect (dashed line)

The reduction effect is introduced through the correction factor, UL_{corr} . When no cancellation is present, UL_{corr} = 1 and when the OL-effect is completely cancelled UL_{corr} = 0. The actual value of the correction factor is in between these extremes and is calculated by Equation 20.

$$UL_{corr} = 1 - c_{UL} \frac{S_{min}^{min} - S_{min}}{\Delta S_{o\ peak}} \tag{20}$$

where c_{UL} is a fitting parameter and S_{min}^{min} is the lowest UL in the current OL influence zone. Multiple ULs, each only slightly smaller than the previous, could conceivably cause unrealistically rapid cancellation of the OL effect. Therefore, a threshold value c_{thres} is included. Cancellation only takes place when $UL_{corr} < c_{thres}$, where c_{thres} is a fitting parameter. It is advised to use 0.95 as cancellation threshold. The UL effect is schematically shown in Figure 14, where ΔS_o is plotted as a function of a for an OL scenario including UL (solid line) and excluding UL (dashed line). The implementation of the UL effect in the SECOD model is shown in Figure 16.

Finally, the assumptions presented above have one exception: the numerical simulation with the Thick Level Set method showed that two large but equal ULs do have a

cumulative cancellation effect. The cancellation effect by the second UL is, however, considerably smaller than by the first. To be able to include this behaviour, the state variable S_{min}^{min} is updated, after the UL effect is determined, according to Equation 21.

$$S_{min}^{min} = S_{min}^{min} - c_{min}(S_{min}^{min} - S_{min}) \tag{21}$$

In which c_{min} is a fitting parameter. The state variable S_{min}^{min} is lowered by a small fraction, c_{min} , of the difference S_{min}^{min} - S_{min} . This way, a second UL with equal S_{min} as the first will still slightly cancel the retardation effect, see Equation 20. The amount of cancellation, UL_{corr} will, however, decrease exponentially with every equally sized UL until it is below the threshold value. Figure 15 gives an overview of the variables used to determine the UL effect. In the following paragraphs, each block from the flowchart is explained.

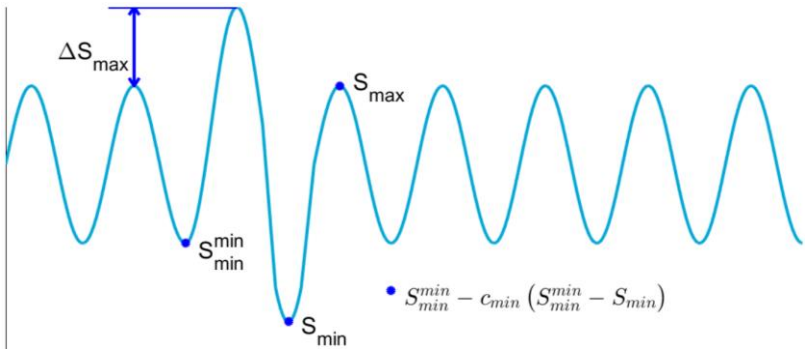

Figure 15: Schematic overview of an OL / UL combination and the correction of S_{min}^{min}

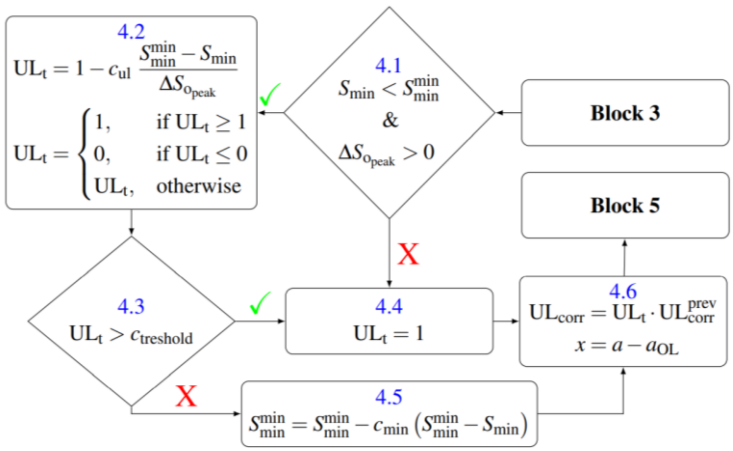

Figure 16: The implementation of an UL

Block 4.1: Is the current cycle an UL?

The current cycle is an UL when the minimum stress of the current cycle, $S_{\min}$, is lower than the lowest minimum stress in the current OL influence zone, $S_{\min}^{\min}$.

Block 4.2: Calculating of the reduction factor based on the current UL

When a new UL is encountered, the correction factor of the current cycle, UL_t, is calculated with Equation 22. It is a function of the ratio between the difference in minimum stress and $\Delta S_{o\,peak}$. This relates the size of the UL to the amount of plasticity that was introduced by the OL.

$$UL_t = 1 - c_{UL}\frac{S_{\min}^{\min} - S_{\min}}{\Delta S_{o\,peak}}$$

$$UL_t = \begin{cases} 1 & \text{if } UL_t \geq 1 \\ 0 & \text{if } UL_t \leq 0 \\ UL_t & \text{otherwise} \end{cases} \tag{22}$$

Block 4.3: Comparing UL_t with the threshold

In case of multiple small ULs, every UL will results in a small correction factor. Adding all these small factors results in an unrealistic large reduction of the retardation effect. Therefore, the threshold c_{thres} is introduced.

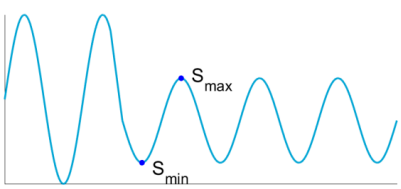

Figure 17a: Schematic representation of the downwards mean change

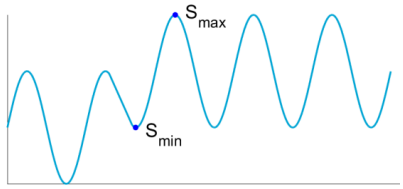

Figure 17b: Schematic representation of the upward mean change

Block 4.4: No cancellation effect

When the current cycle does not meet the criteria for an UL, or does not exceed the threshold value c_{thres}, the correction factor UL_t is set to 1. This means that there is no cancellation included for the current cycle.

Block 4.5: Updating $S_{\min}^{\min}$

To include the effect of multiple large ULs, $S_{\min}^{\min}$ is corrected according to Equation 21.

Block 4.6: Calculating total UL correction factor UL_{corr}

A cumulative correction factor is determined as state variable, covering the combined cancellation effect of all ULs:

$$UL_{\text{corr}} = UL_{\text{t}} \cdot UL_{\text{corr}}^{\text{prev}} \tag{23}$$

Furthermore, the crack length since overload is updated:

$$x = a - a_{\text{OL}} \tag{24}$$

Block 5: Detecting upward mean changes

Block 5 handles a special but important exception: the mean change upwards. This subsection first provides an overview of this mean change and the implementation, after which the flowchart for block 5 is presented and discussed block-by-block.

The effect of mean changes

Two types of mean change have been defined, downwards and upwards, see Figure 17. A downward mean change is characterized by a decrease in S_{max} , which is recognized by block 3 as an OL event of the previous cycles. If S_{min} (also) decreases, this is included as UL by block 4. The combined effect provides the response to a downward mean change. An upward mean change, on the contrary, does not introduce any OL or UL events and can thus be treated as a separate load cycle. However, with one exception is defined: when the upward mean change occurs within the OL influence zone.

In this special case, an increasing mean shift will cause a higher S_{o} due to the increase in the steady state opening stress (the opening stress of the current cycle, without OL or UL effects) S_{oss} as shown in Figure 18. The figure shows an OL with an upward mean change applied when the retardation effect is decaying. This mean change will cause an increase of the steady state crack opening stress S_{oss} . However, ΔS_{o} remains unchanged, as it is a function of the OL, such that the total opening stress will increase (see blue curve in Figure 18). From a physical point of view this is not feasible, because this would mean that an increasing mean change will also increase the amount of plasticity in the wake of the crack and thus the amount of retardation. Alternatively, forcing S_{o} to remain unchanged provides a situation where the retardation zone is shortened dramatically and this introduces a much shorter OL influence zone (dashed line). To overcome this, a new (artificial) OL is determined, with a plastic zone size edge that coincides with the original

plastic zone edge and with the new S_{oss} as baseline. This will reduce the amount of retardation, without shortening the influence zone (dash-dot line).

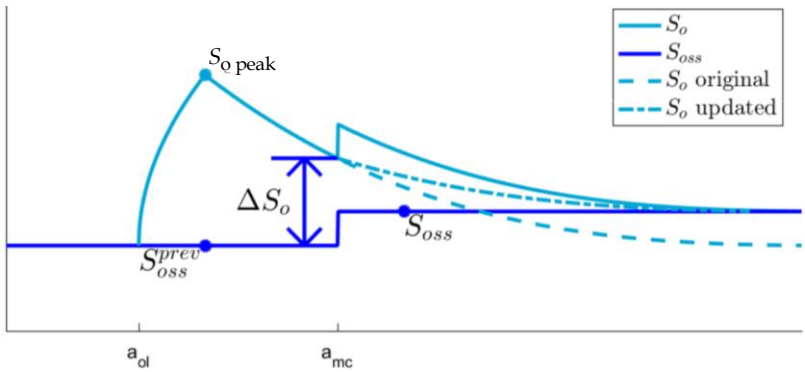

Figure 18: The effect of an increasing mean shift in the OL-influence zone

The new OL effect is introduced in such a way that the crack starts at x_{top} of the new plastic zone. This is illustrated in Figure 19 by a green line. This approach avoids inclusion of a second delayed retardation phenomenon and ensures a smooth ΔS_o curve. This is explained in more detail with the following equations, in which the superscript *b* and *g* represent the previous (blue) OL event and the new (green) event, respectively. First, the new plastic zone size is created based on the previous plastic zone size and the current position, x:

$$r_{OL}^{g} = \frac{r_{OL}^{b} - x^{b}}{1 + c_{top}} \tag{25}$$

Subsequently, a new x, x_{top} and a_{OL} can be determined:

$$x_{top}^{g} = c_{top} \cdot r_{OL}^{g} \tag{26}$$

$$a_{OL}^{g} = a^{prev} - x_{top}^{g} \tag{27}$$

$$x^{g} = a^{prev} - a_{OL}^{g} \tag{28}$$

A new value for the maximum openings stress $\Delta S_{o\ peak}$ is determined based on the previous and current opening stress, as shown schematically in Figure 19.

$$\Delta S_{o\ peak} = \Delta S_{o}^{prev} - \Delta S_{o} \tag{29}$$

The procedure is summarized in Figure 20 and is explained block by block in the next paragraphs.

Block 5.1: Is an increasing mean change present within an OL event?

This decision block detects upward mean changes ($S_{max} > S_{max}^{prev}$) and checks whether or not a retardation effect is present, ($\Delta S_o \geq 0$).

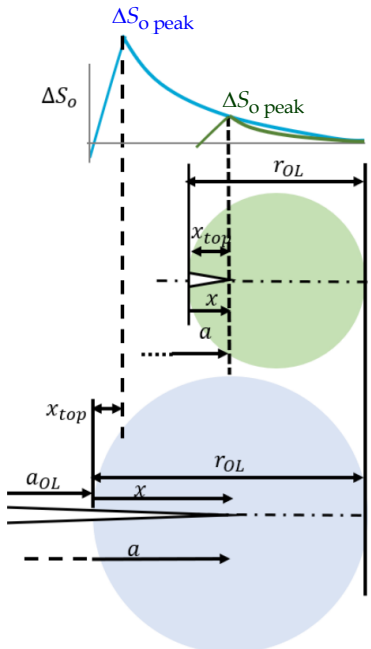

Figure 19: Schematization of new calculated plastic zone in case of a mean shift

Block 5.2: Calculating ΔS_o

In case of a mean shift, the associated increase in S_{oss} is calculated. This value is called ΔS_{oss} and used in blocks 5.4 and 5.5.

Block 5.3: Is the current cycle within a delayed retardation regime ($x < x_{top}$)?

Similarly to block 3.4, the distinction is made between the delayed retardation ($x < x_{top}$) or regular decaying retardation zones ($x \geq x_{top}$).

Block 5.4: Determining the equivalent OL ($x \geq x_{top}$)

This block calculates the new OL.

Block 5.5: Determining the equivalent OL ($x < x_{top}$)

When the mean change takes place in the acceleration or delayed retardation phase, the value for $\Delta S_{o\ peak}$ is lowered by the increase in steady state opening stress ΔS_o, to avoid the increase in peak opening stress.

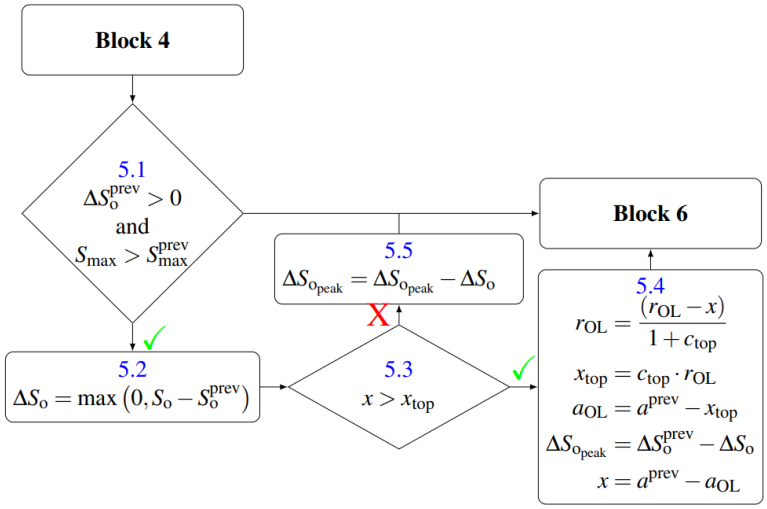

Figure 20: Correction for upward mean changes during the OL effect

Block 6: Calculating the crack growth

Block 6 calculates the crack growth for the current cycle, taking the possible OL and UL effects into account. First, the implementation of the crack growth equations is explained, after which each separate block is elaborated upon.

Calculating the crack growth

The crack growth depends on whether or not an OL effect is present. When present, the shape function equations (Equations 12 and 13) are used to determine ΔS_o and thus the current crack opening stress $S_o = S_{oss} + \Delta S_o$. Otherwise, when no OL effect is present, $\Delta S_o = 0$ and $S_o = S_{oss}$. This is used to calculate the opening stress intensity factor K_o and the effective stress intensity factor, ΔK_{eff}:

$$K_o = Y S_o \sqrt{\pi a} \tag{30}$$

$$\Delta K_{eff} = K_{max} - \max(K_o, K_{min}) \tag{31}$$

With ΔK_{eff}, the crack growth is determined using the following equation in which $C_{eff} = \frac{C}{U_{ss}^m}$:

$$\frac{da}{dN} = C_{eff} (\Delta K_{eff})^{meff} \tag{32}$$

Finally, the total crack length can be updated (as this is done every cycle, $N = 1$):

$$a = a^{prev} + \frac{da}{dN} \Delta N \tag{33}$$

The entire procedure is visualized in Figure 21 and is explained in the next paragraphs.

Block 6.1: Is an OL effect present?

To make sure the correct opening stress equations are used, a check is performed to see whether or not any OL effects are present.

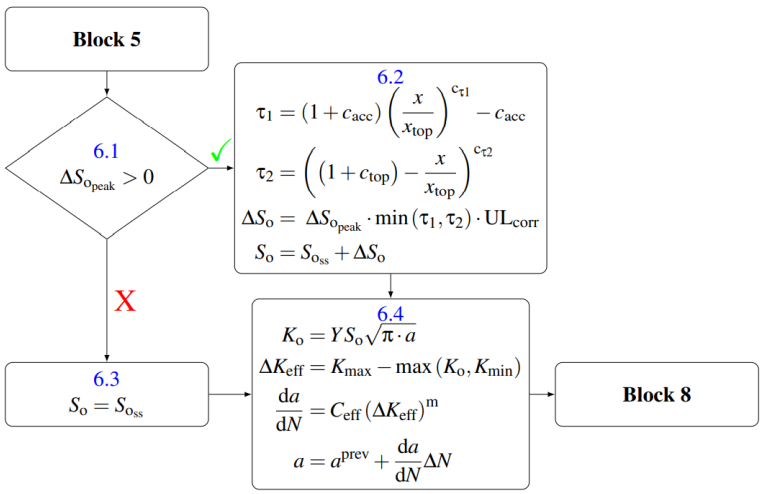

Figure 21: Calculation of the crack growth

Block 6.2: Calculating the opening stress in case an OL effect is present

Using the shape functions of the OL description, the opening stress (S_o) is calculated.

Block 6.3: Calculating the opening stress in case no OL effect is present

When no OL effect is present, $\Delta S_o = 0$ and the steady state opening stress, $S_{o\,ss}$ is used to determine the crack growth.

Block 6.4: Calculating the effective stress intensity factor and crack growth

The final step is to determine the effective stress intensity factor, ΔK_{eff} , based on the opening stress, S_o . Then, the crack growth per cycle is determined and the total crack length is updated (for every cycle, thus $\Delta N = 1$).

Block 7: Checking for compressive ULs

Whenever a cycle is in full compression, $K_{max} < 0$, it is assumed that there is no crack growth. However, if this cycle is still an UL it can reduce the amount of retardation in the

system. Therefore block 4 is repeated in this part and the state variables describing the UL effect (i.e. $S_{\min}^{\min}$ and UL_{corr}) are updated for use at a subsequent cycle.

Block 8: Preparing for the next cycle

The final block saves all relevant state variables so they can be used with the next cycle. Furthermore, this block is also used to save parameters to a suited output format. An overview of the state variables used by the SECOD model is given in Table 1.

5 Comparison with experiments

Numerous small scale four-point-bending (SENB4) fatigue tests are used to develop and calibrate the SECOD model. These experiments are described by Pijpers et al. (2019). First, a short summary is given of the experimental set-up. Second, the calibration procedure for the SECOD model is discussed. Finally, the effectiveness of the SECOD model is showed by comparing the results from the SECOD model with the results from the experiments and the predictions from the State-Space and Willenborg models.

Table 1: Overview of state variables

State variable	Governs effect of
$\Delta K_{\min}^{\text{prev}}$	Minimum stress intensity of the previous cycle
$\Delta K_{\max}^{\text{prev}}$	Maximum stress intensity of the previous cycle
$\Delta S_{o}^{\text{prev}}$	Value of the opening stress of the previous cycle
$\Delta S_{o\ \text{peak}}$	Peak openings stress in the OL influence zone
a	Crack length
r_{OL}	Length of OL influence zone
$S_{\max}^{\text{prev}}$	Maximum stress of the previous cycle
$S_{\min}^{\min}$	Lowest $S_{\min}$ in the current OL influence zone
UL_{corr}	UL correction factor
x_{top}	Location of $S_{\max}^{\text{prev}}$ relative to the OL event
x_{OL}	Length of the OL influence zone

5.1 Description of the experimental set-up

The experimental set-up for the small scale fatigue tests, as described by Pijpers et al. (2019), was built at the TNO Structural Dynamics Lab in Delft. The set-up consists of standard SENB4 single edge notched specimens in four-point bending, made of S355G10+M base material. The SENB4 specimens are 25 mm wide and have a height of 50 mm. The specimen is loaded by a hydraulic cylinder and is supported by rollers, with a distance between them of 140 mm and 280 mm. These dimensions are chosen such that local plasticity at the roller is avoided. The test set-up is shown in Figure 22.

The loading is applied at a frequency of 4 Hz and the applied loading is measured, together with the crack propagation. The latter is monitored with Vishay crack gauges, with a 0.25 mm spacing (see Figure 22). In addition, visual methods are used to estimate the crack length at discrete intervals.

This paper uses a subset of the entire experimental program discussed by Pijpers et al. (2019) for comparison with the SECOD model, see Table 2. Because only a limited set of

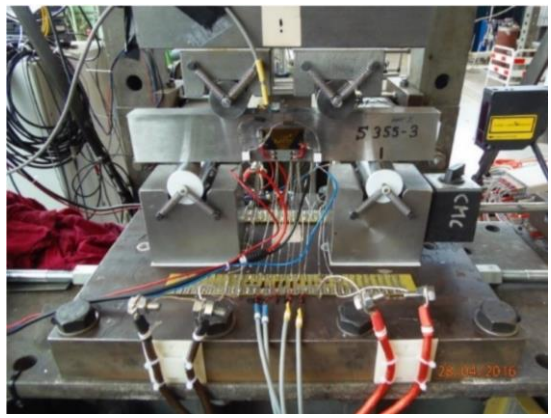

Figure 22: Side view of the SENB4 specimen, including instrumentation

Table 2: Overview of tests discussed in this paper

Specimen ID	Signal type
BM1235	CA loading with OL-UL combinations
BM1535	CA loading with OL events
BM1735	CA loading blocks with OL and mean changes
BM2535	CA loading with OL and OL-UL combination

experiments is available, these four are used to calibrate the SECOD model and also to show the merits of using it. For future work, it is recommended to expand the experimental program and use these new experiments for 'blind validation' purposes.

5.2 Calibration SECOD model

The model parameters have been calibrated using the following experiments:

1. CA

The material parameters C and m are based on CA tests or parts of the signal that feature CA signal without being in the OL or UL influence zone.

2. CA + OL

The retardation zone parameters, c_{top} ; c_x ; $c_{\tau 1}$ and $c_{\tau 2}$ are calibrated based on CA + OL signals by fitting the OL influence zone to the experimentally determined one. When multiple OL-ratios are available, these can be used to fit calibration factors c_1 and c_2 .

3. CA+OL+UL

A block type signal is used to calibrate c_{acc} and c_{UL} . When multiple UL are available, these can be used to calibrate c_{min} .

4. VA

A VA loading signal can be used to calibrate the threshold value c_{thres} .

This calibration has resulted in the model properties described in Table 3 and Table 4. A two stage crack growth versus stress intensity description is used, providing two sets of parameters, C_1 and m_1 for relatively small stress ranges and C_2 and m_2 for larger stress cycles. The constant amplitude crack growth rate is: $da/dN = \min(C_1 \Delta K^{m1} ; C_2 \Delta K^{m2})$. In order to provide the most accurate crack growth estimation for each specimen, the parameters C_1 ; C_2 ; m_1 and m_2 have been determined for each of the specimens, instead of an average value for all specimens.

5.3 Calibration other models

The three analytical models, the crack growth without any OL and UL effects, the Generalized Willenborg model and the State-Space model are calibrated to fit the experiments. To start with, all three models use the crack growth parameters that are determined based on the experiments (see Table 4). For the first model, the crack growth representation without OL and UL effects, no further calibration is required. Secondly the Generalized Willenborg model, which does not allow for further calibration and solely

Table 3: Overview of calibration parameters

Factor	Governs the effect of	Value
c_1	Difference between S_{max}^{ss} and S_{max}^{OL} on S_o	0.65
c_2	Ratio between S_{max}^{ss} and S_{max}^{OL} on S_o	0.43
c_{acc}	Initial acceleration	0.05
c_{min}	Correction for large ULs	0.90
c_{top}	Location of maximum retardation peak	0.05
c_{UL}	Cancelling effect of an UL	0.19
c_{thres}	Threshold value for the UL effect	0.95
c_x	Length of the influence zone	0.14
$c_{\tau 1}$	Increase function of ΔS_o	0.50
$c_{\tau 2}$	Decay function of ΔS_o	3.00

Table 4: Overview of material parameters for all specimens (using a two-stage crack growth

Specimen ID	a_0	C_1	m^1	C_2	m^2
BM1235	2.5	$6.5 \cdot 10^{-17}$	4.3	N/A	N/A
BM1535	2.5	$1.8 \cdot 10^{-16}$	4.2	$3.3 \cdot 10^{-8}$	1.3
BM1735	2.5	$4.6 \cdot 10^{-18}$	5.0	$1.1 \cdot 10^{-9}$	1.8
BM2535	4.0	$1.8 \cdot 10^{-16}$	4.2	$3.3 \cdot 10^{-8}$	1.3

For all specimens: q = 1.0 and p = 0.2

depends on the ratio of the OL to the CA cycles and the constraint parameters. Finally, the State-Space model does allow for further calibration through the decay parameter η, which controls length and magnitude of the retardation effect, see Equation 10, Section 2. For the following analysis, this parameter has been fitted such that the length of the OL zone (in terms of da/dN over crack growth) fits best with the experiments. Unfortunately, a single value for η proved insufficient to properly fit all measurement data.

*5.4 **Validation with the experiments***

Each of the four experiments used to validate the model contains CA loading with variations in the events: a) two OLs (BM1535), b) two OL-UL combinations (BM1235), c)

OL and OL-UL combination (BM2535) and d) OL followed by various mean shifts (BM1735). The comparison with the analytical models is visualized in Figures 23 through 26. On the left side of these figures, the crack growth versus the number of cycles is shown. The second y-axis shows the stress input and corresponds to the grey lines in the figure. These represent the upper and lower bounds of the input signal, as actual loading is sinusoidal. The black curve represents the crack growth without taking any OL and UL effects into account. The coloured curves represent the retardation models: Generalized Willenborg model (green), State-Space model (red) and SECOD model (blue). The experimental data are indicated with crosses at 0.25 mm crack growth intervals. The crack growth at the location of the OL is (also) estimated visually.

To make the models easier to compare, the events (OLs, ULs and mean changes) have been applied in the models at set crack sizes (e.g. a = 5.5 mm). This means that cumulative errors may occur when considering the crack growth over number of cycles. This is, however, not the case for the crack growth per cycle da/dN versus crack length, which is shown on the right side of Figures 23 through 26. This figure provides insight into the estimated crack growth and especially into the behaviour after an event is included. The following paragraphs discuss the results for each experiment separately.

Two OLs

Figure 23 shows the results of specimen BM1535. This specimen features a CA loading with an R-ratio of 0.3 and two discrete OL effects. The experimental results clearly show initial acceleration behaviour, directly followed by distinct retardation zones. The final part of the loading signal is again CA loading. The figure demonstrates that the SECOD model follows the experimental data well, providing a slightly conservative estimation of the crack growth over the number of cycles. Both the Generalized Willenborg and State-Space models underestimate the crack growth behaviour, but the mechanism is different, as is shown in the right-hand graph of Figure 23. The length of the retardation zone is underestimated in the Generalized Willenborg model. This means that the crack growth rate has returned to the CA values long before this is the case in the experiment. The peak value, however, is in line with the experimental values. On the other hand, the peak value is underestimated in the State-space model, but the retardation zone is much longer than experimentally determined.

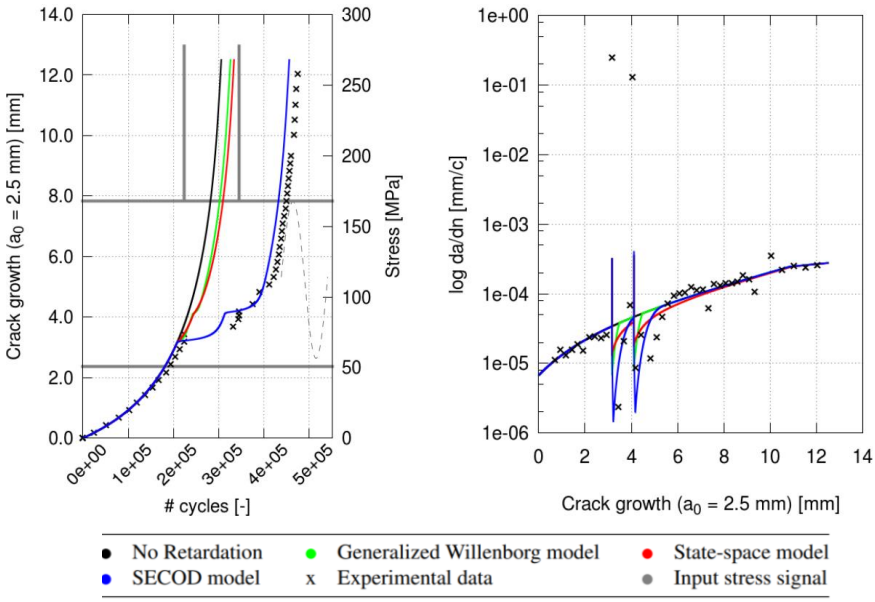

Figure 23: Specimen BM1535, showing crack growth versus number of cycles (left) and crack growth per cycle versus crack length (right)

Two OL-UL combinations

The second experiment is specimen BM1235, see Figure 24. This specimen features CA loading, combined with two sets each containing an OL directly followed by an UL. Furthermore, the two OL have a different OL-ratio, while both ULs are equal. The OLs are immediately followed by the ULs. The SECOD model follows the first OL/UL combination well and underestimates the retardation induced by the second combination. Similar to specimen BM1535, the Generalized Willenborg model estimates the magnitude of the retardation effect reasonably well, but underestimates the length of the retardation zone. This leads to an underestimation of the retardation effect. It should be noted that this behaviour is partially attributed to the fact that the Generalized Willenborg model does not include the UL effect: Figure 24 therefore provides a too optimistic representation of the accuracy of the Generalized Willenborg model. The State-Space model does include the cancellation effect induced by the UL, but overestimates the cancellation effect, resulting in a severe underestimation of the final retardation effect.

OL and OL-UL combination

Figure 25 shows the results from specimen BM2335. This is an interesting specimen, as the combination of a single OL and the OL/UL combination clearly show the effect of an UL

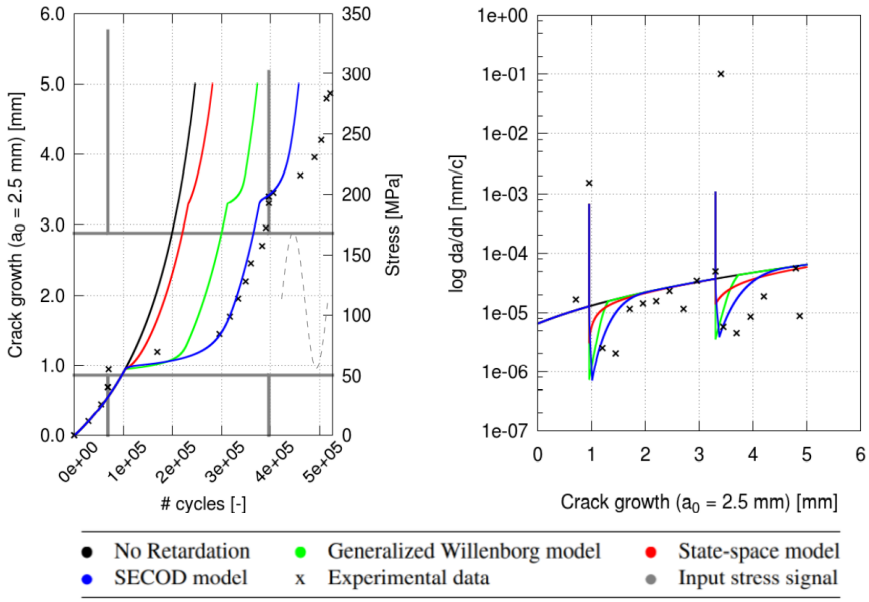

Figure 24: Specimen BM1235, showing crack growth versus number of cycles (left) and crack growth per cycle versus crack length (right)

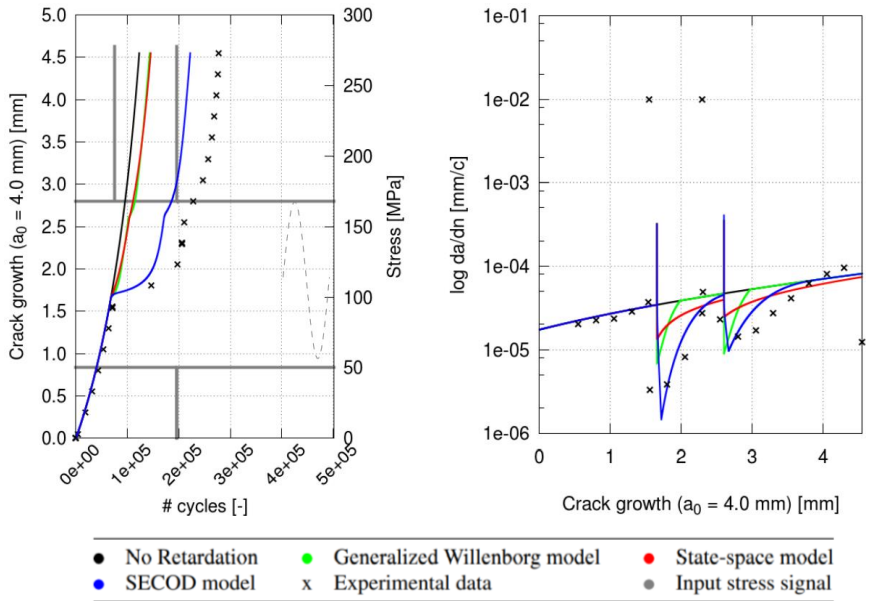

Figure 25: Specimen BM2535, showing crack growth versus number of cycles (left) and crack growth per cycle versus crack length (right)

on the net retardation effect. The retardation effect of the OLUL combination is much smaller, compared to that of the single OL event. The SECOD model predicts a slightly smaller retardation effect than the experimental data for both events. Again, both the Generalized Willenborg model and the State-Space model severely underestimate the retardation effect due to their mismatch of the magnitude and length of the retardation zone, respectively.

OL and mean changes

The most complicated signal has been tested with specimen BM1735 and shown by Figure 26. An OL is followed by a series of mean changes. Comparison of the experiments with the No Retardation approach shows that both the OL and the downward mean changes induce retardation. The SECOD model is able to reasonably follow this complicated signal, with the exception of the first mean change which is not captured well. This results in a cumulative error over the remainder of the signal. The mismatch at the first mean change is attributed to a particular combination of S_o and R-ratio. This makes that the SECOD model provides a worse overall fit than the State-Space for this experiment. However, the right-hand graph provides a different picture. Similarly to the other experiments, the State-Space model overestimates the length of the retardation zone whereas the SECOD model

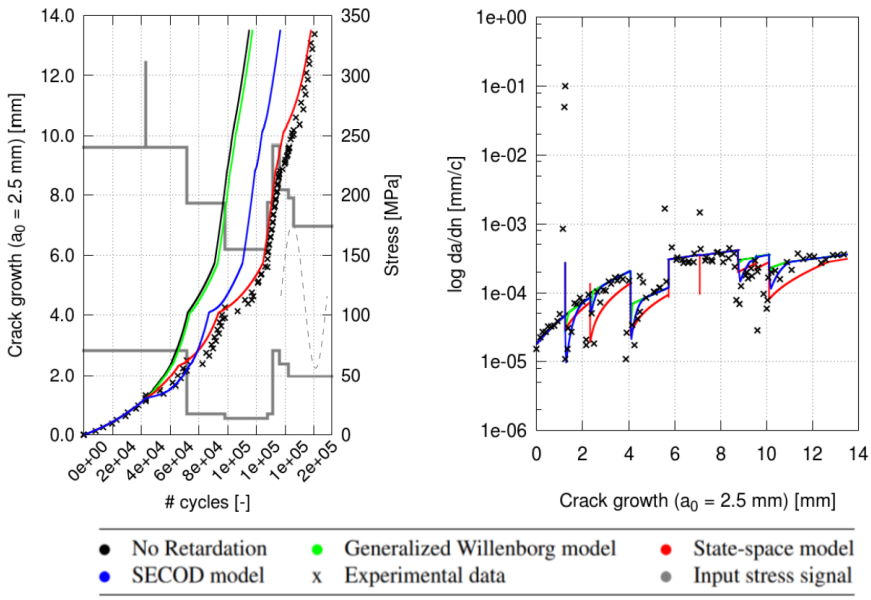

Figure 26: Specimen BM1735, showing crack growth versus number of cycles (left) and crack growth per cycle versus crack length (right)

follows the experimentally determined *da/dN* curve with reasonable accuracy. The Generalized Willenborg model predicts almost no retardation effect.

6 Discussion new SECOD model

The SECOD model shows reasonably to good agreement with the four experiments it has been compared against. It provides a decent match over a range of *R*-ratios and OL/UL effects. Furthermore, it provides a more uniform match than the Generalized Willenborg or State-Space models, which can be fitted to a particular experiment but if so, do show large differences with the other ones. In this section, the key features and limitations of the SECOD model are discussed.

Pattern of the opening stress

The basis of the SECOD model is a set of equations describing the decrease, increase and again decrease of the opening stress caused by a single OL, causing initial acceleration and (delayed) retardation of the crack growth rate. The figures presented above show the effectiveness of this approach, as the OL effect is captured rather well over the whole range of experiments performed.

The shape of the OL influence zone scales well with the events presented, both in terms of the magnitude of the retardation effect and the length of the influence zone. Generally, the current description is conservative in comparison with the experiments, underestimating the retardation effect.

The UL effect

The current set of experiments contains a number of discrete ULs, the effect of which is captured reasonably well by the SECOD model. Furthermore, due to the description of the model, the UL can be applied at any given moment providing the flexibility required to describe (semi-) VA signals. This is a big benefit compared to, for example, the State-Space model, where the UL must follow the OL directly.

Mean changes

Figure 26 shows that mean changes introduce a net retardation effect which is captures reasonably well by the SECOD model. This provides confidence in the chosen approach to combine OL and UL effects separately. Again, this opens the possibility to describe (semi-) VA signals.

VA loading

From the start, the SECOD model has been developed with VA loading in mind. Due to the modular design, each of the four defined events (CA, OL, UL and mean changes) can be included in an arbitrary manner. This flexibility is achieved through use of state variables to capture the history and by predefining the shape of the OL effect. Finally, the decoupling between the OL and UL effects allow for arbitrary inclusion of either one of them.

This is illustrated by the following example: When an OL is directly followed by an UL, it should provide a very similar crack growth as when the same OL is followed by several small CA cycles and the UL. In terms of the physical processes, the inclusion of several small cycles will cause negligible crack growth and will not reduce of the plasticity in the wake of the crack. Such, the crack growth after both event should be almost the same. The current model approach allows for this behaviour and thereby the arbitrarily inclusion of OL and UL. Furthermore, as mean changes consists of a combined OL/UL effect, the same reasoning holds for these events.

Limitations of the SECOD model

The SECOD model has been calibrated based on a limited set of experiments, thereby inherently limiting the application area in which the model is valid. More tests are required to validate the model for a wider range of loading conditions. These calibration and validation experiments are recommended to include VA signals, to check the validity of the method for these as well. The main challenge when testing VA signals is the measurement resolution of the crack growth. Currently, it is not possible to measure the crack growth with sufficient accuracy to trace individual events during a VA loading. This makes that it is only possible to validate for general trends, but not to improve on the crack growth due to specific combinations of stress cycles.

The SECOD model has been developed and calibrated for base material tests. However, the focus for fatigue of practical structures are welded details, as this is the part of the structure where fatigue cracks normally initiate. In this area, large pre-stresses, due to the welding process, are present and will influence the fatigue behaviour. The current model allows for inclusion of pre-stresses (as a function of the crack length) to $S_{\min}$ and $S_{\max}$ but the model needs to be validated based on a similar set of experiments, performed on welded specimens.

7 Conclusions

The Simple Equation based Crack Opening Determination (SECOD) model is developed to estimate the fatigue crack growth rate in steel, including retardation and acceleration effects caused by (combinations) of Overload (OL)s and Underload (UL)s. The model is developed in a modular fashion, such that it can facilitate (semi-)Variable Amplitude (VA) loading histories. This analytical model is developed by using a combination of numerical simulations and crack growth experiments. The main idea behind the SECOD model is a set of scaleable equations that describe the effect of an OL on the crack opening stress and the cancellation of the retardation effect associated with ULs. By treating the OLs and ULs separately, the model has the potential to describe realistic, VA load patterns.

The SECOD model has been calibrated to a set of experiments. It simulates the crack growth with reasonable accuracy. Compared to similar analytical models, it provides better accuracy over a wider range of loading conditions.

For future work, it is recommended to further generalize and validate the model for a larger set of loading conditions, through more experiments. Similarly, based on experimental data, the model parameters can be calibrated for welded details and include pre stress.

References

Anderson, T. L. (2017). *Fracture mechanics: fundamentals and applications*. CRC press.

Ding, Z.,Wang, X., Gao, Z., and Bao, S. (2017). An experimental investigation and prediction of fatigue crack growth under overload/underload in q345r steel. *International journal of fatigue*, 98:155–166.

Dragt, R., Allaix, D., Maljaars, J., Tuitman, J., Salman, Y., Otheguy, M., et al. (2017). Approach to include load sequence effects in the design of an offshore wind turbine substructure. In The 27th *International Ocean and Polar Engineering Conference*. International Society of Offshore and Polar Engineers (ISOPE), San Francisco USA, June 25-30.

Dragt, R., Hengeveld, S., and Maljaars, J. (2018). A new model for fatigue load sequence effects in offshore wind turbine substructures and its implications for design life. In The 28th *International Ocean and Polar Engineering Conference*, ISOPE, Sapporo, Japan, June 10-15.

Dragt, R., Maljaars, J., Tuitman, J., Salman, Y., Otheguy, M., et al. (2016). Including load sequence effects in the fatigue damage estimation of an offshore wind turbine substructure. In The 26th *International Ocean and Polar Engineering Conference*. International Society of Offshore and Polar Engineers.

Elber, W. (1971). The significance of fatigue crack closure. In Damage tolerance in aircraft structures. *ASTM International*. ed. M. Rosenfeld, pp. 230-242.

Gallagher, J. (1974). A generalized development of yield zone models. Technical report, Wright-Patterson: Air Force Flight Dynamics Laboratory.

Koc¸ak, M., Hadley, I., Szavai, S., Tkach, Y., and Taylor, N. (2008). Fitnet fitness-for-service (ffs) procedure-volume 1, revision mk8. Joint Research Centre, GKSS Research Centre Geesthacht.

Maljaars, J., Pijpers, R., and Slot, H. (2015). Load sequence effects in fatigue crack growth of thick-walled welded c–mn steel members. *International Journal of Fatigue*, 79:10–24.

Maljaars, J. and Tang, L. (2019). How the finite element method helps explaining fatigue crack growth retardation and acceleration. *HERON*. Vol. 65 (2020) No. 1/2 pp. 69-108

Nip, K., Gardner, L., Davies, C., and Elghazouli, A. (2010). Extremely low cycle fatigue tests on structural carbon steel and stainless steel. *Journal of constructional steel research*, 66(1):96–110.

Paris, P. C. (1964). *The fracture mechanics approach to fatigue*.

Pijpers, R., Verdenius, S., Abspoel-Bukman, L., and Maljaars, J. (2019). Fatigue crack growth retardation and acceleration in coupon specimens and tubular joint element specimens. *HERON*. Vol. 65 (2020) No. 1/2 pp. 5-67

Ray, A. and Patankar, R. (2001). Fatigue crack growth under variable-amplitude loading: Part i–model formulation in state-space setting. *Applied Mathematical Modelling*, 25(11):979–994.

Tada, H., Paris, P., and Irwin, G. (1973). *The stress analysis of cracks*. Handbook, Del Research Corporation.

Toribio, J. and Kharin, V. (2013). Simulations of fatigue crack growth by blunting–resharpening: plasticity induced crack closure vs. alternative controlling variables. *International Journal of Fatigue,* 50:72–82.

Voormeeren, L., van der Meer, F., Maljaars, J., and Sluys, L. (2017). A new method for fatigue life prediction based on the thick level set approach. *Engineering Fracture Mechanics*. Vol. 182, Sept. 2017, pp. 449-466.

Willenborg, J., Engle, R., and Wood, H. (1971). A crack growth retardation model using an effective stress concept. Technical report, AIR FORCE FLIGHT DYNAMICS LAB WRIGHT-PATTERSON AFB OH.

Yisheng, W. and Schijve, J. (1995). Fatigue crack closure measurements on 2024-t3 sheet specimens. *Fatigue & Fracture of Engineering Materials & Structures*, 18(9):917–921.

Yuen, B. and Taheri, F. (2006). Proposed modifications to the wheeler retardation model for multiple overloading fatigue life prediction. *International journal of fatigue*, 28(12):1803–1819.